



CHORUS

This is the accepted manuscript made available via CHORUS. The article has been published as:

## Chained Bell Inequality Experiment with High-Efficiency Measurements

T. R. Tan, Y. Wan, S. Erickson, P. Bierhorst, D. Kienzler, S. Glancy, E. Knill, D. Leibfried, and D. J. Wineland

Phys. Rev. Lett. **118**, 130403 — Published 28 March 2017

DOI: [10.1103/PhysRevLett.118.130403](https://doi.org/10.1103/PhysRevLett.118.130403)

# Chained Bell Inequality Experiment with High-Efficiency Measurements

T. R. Tan,<sup>1,2,\*</sup> Y. Wan,<sup>1</sup> S. Erickson,<sup>1,2</sup> P. Bierhorst,<sup>1</sup> D. Kienzler,<sup>1</sup>  
S. Glancy,<sup>1</sup> E. Knill,<sup>1,3</sup> D. Leibfried,<sup>1</sup> and D. J. Wineland<sup>1,†</sup>

<sup>1</sup>*National Institute of Standards and Technology, 325 Broadway, Boulder, Colorado 80305, USA*

<sup>2</sup>*Department of Physics, University of Colorado, Boulder, Colorado 80309, USA*

<sup>3</sup>*Center for Theory of Quantum Matter, University of Colorado, Boulder, Colorado 80309, USA*

We report correlation measurements on two  ${}^9\text{Be}^+$  ions that violate a chained Bell inequality obeyed by any local-realistic theory. The correlations can be modeled as derived from a mixture of a local-realistic probabilistic distribution and a distribution that violates the inequality. A statistical framework is formulated to quantify the local-realistic fraction allowable in the observed distribution without the fair-sampling or independent-and-identical-distributions assumptions. We exclude models of our experiment whose local-realistic fraction is above 0.327 at the 95 % confidence level. This bound is significantly lower than 0.586, the minimum fraction derived from a perfect Clauser-Horne-Shimony-Holt inequality experiment. Furthermore, our data provides a device-independent certification of the deterministically created Bell states.

Recently several groups have reported loophole-free tests of local realism with Bell’s theorem [1], rejecting with high confidence theories of local realism [2–4]. While these experiments falsify the idea that nature obeys local realism, they are limited in the extent to which their data differs from local realism. Chained Bell inequality (CBI) [5] experiments can show greater departures from local realism in the following sense: Elitzur, Popescu, and Rohrlich [6] described a model of the distribution of outcomes measured from a quantum state as a mixture of a local-realistic distribution, which obeys Bell’s inequalities, and another distribution that does not. Following their convention, we call these distributions “local” and “non-local.” According to Ref. [6], a probability distribution  $P$  for the outcomes of an experiment can be written as

$$P = p_{\text{local}}P^L + (1 - p_{\text{local}})P^{NL}, \quad (1)$$

where  $P^L$  represents a local joint probability distribution (a “local part”) and  $P^{NL}$  represents a non-local distribution, with  $p_{\text{local}}$  as the weight of the local component bound by  $0 \leq p_{\text{local}} \leq 1$ . For an ideal Clauser-Horne-Shimony-Holt (CHSH) Bell inequality experiment where two physical systems (usually particles) are jointly measured with four different measurement settings [7], the lowest attainable upper bound on the local content  $p_{\text{local}}$  in any quantum distribution is  $\sim 0.586$  [8, 9]. In principle, this bound can be lowered to zero by using a chained Bell inequality experiment.

As indicated in Fig. 1, CBI experiments are similar to CHSH-type experiments, but involve more measurement settings. During each trial, a source that may be treated as a “black box” emits two systems labeled  $a$  and  $b$ , respectively. The experimentalist records the measurement outcomes after choosing a pair of measurements to perform separately on  $a$  and  $b$ . We use the symbols  $a_k$ ,  $b_l$  to denote the respective measurement settings and  $a_k b_l$  for the pair. The latter is usually simply referred to as “the settings” or “the setting pairs”. There is a hierarchy

in which the  $N$ th CBI experiment involves  $2N$  different settings. The  $N = 2$  CBI experiment is equivalent to the CHSH Bell inequality experiment. The settings for general  $N$  are chosen from the set

$$Z = \{a_1 b_1, a_1 b_2, a_2 b_2, a_2 b_3, \dots, a_{N-1} b_N, a_N b_N, a_N b_1\}. \quad (2)$$

Each local measurement has a binary outcome of  $B$  for “bright” or  $D$  for “dark” (Fig. 1). The outcome of the trial is recorded as  $c(x, y) = 1$  if  $x = y$  or 0 if  $x \neq y$ , where  $x$  is the outcome from system  $a$  and  $y$  is the outcome from system  $b$ . The probability to obtain  $c(x, y) = 1$  may depend on the choices  $a_k$  and  $b_l$ , so we define that probability to be the correlation  $\mathcal{C}(a_k, b_l) = P(BB|a_k b_l) + P(DD|a_k b_l)$ , where  $P(xy|a_k b_l)$  is the probability that system  $a$  yields measurement outcome  $x$  and system  $b$  yields measurement outcome  $y$  when the setting pair is  $a_k b_l$ . We define the chained Bell parameter to be:

$$I_N = \mathcal{C}(a_1, b_1) + \mathcal{C}(a_1, b_2) + \mathcal{C}(a_2, b_2) + \dots \\ \dots + \mathcal{C}(a_N, b_N) + (1 - \mathcal{C}(a_N, b_1)). \quad (3)$$

If the experiment is governed by a local hidden variable model, then the CBI  $I_N \geq 1$  must be satisfied [5]. Note that  $I_N$  can be estimated using only the record of the settings  $a_k b_l$  and outcomes  $c(x, y)$ , without knowledge of the mechanism of the source. It was shown in Ref. [8] that the chained Bell parameter  $I_N$  is always an upper bound on  $p_{\text{local}}$ . In fact,  $I_N$  is a least upper bound for  $p_{\text{local}}$  under the assumption that the distributions are non-signaling, in the sense that each party’s measurement outcomes do not depend on the other party’s setting choice [10]. In the limit of  $N \rightarrow \infty$  and with perfect experimental conditions, CBI experiments could be used to show that  $p_{\text{local}} \rightarrow 0$ , demonstrating complete departure from local realism.

Similar to a CHSH-type experiment, a CBI experiment may be subject to “loopholes” [11, 12] that, in principle, allow local systems to show violation of the inequal-

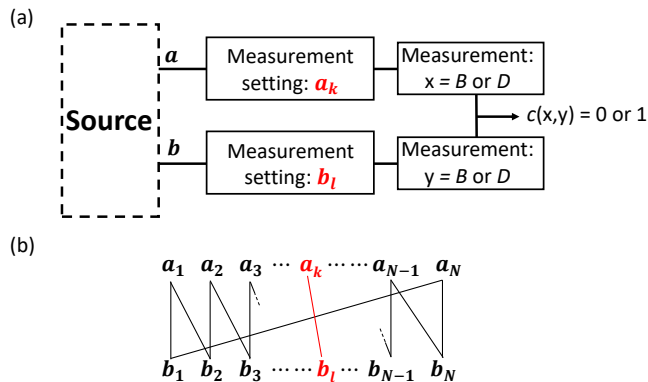


FIG. 1. (a) Illustration of a single trial in a Bell inequality experiment. To begin, a source creates two entangled systems  $a$  and  $b$ , here two  ${}^9\text{Be}^+$  ions. After choosing this trial’s measurement settings  $a_k$  and  $b_l$ , each ion’s state is rotated by an amount corresponding to its settings (which is controlled with classical variables). Then, a standard fluorescence based measurement in a fixed basis is applied to each ion. This is equivalent to choosing the measurement basis for the state that is present before the measurement settings are applied. Each system’s measurement outcome is labeled  $B$  for “bright” or  $D$  for “dark”, corresponding to the observation of fluorescence or not. From the joint measurement we record “ $c = 1$ ” if the outcomes are the same and “ $c = 0$ ” if they are not. (b) “Chaining” of the measurement settings for the  $N$ th CBI experiment. The measurement settings can be visualized as a chain where  $a_k b_k$  and  $a_{k+1} b_{k+1}$  are linked by  $a_k b_{k+1}$ , and the chain is closed by the settings  $a_N b_1$ . Example settings  $a_k$  and  $b_l$  are highlighted in red. The CHSH Bell inequality experiment corresponds to the special case of  $N = 2$ . A full experiment involves many trials with different choices for measurement settings.

ity. These loopholes arise when one must rely on various supporting assumptions that are made in the design and execution of the experiments, but which cannot be absolutely verified. For example, if the setting choice for  $a$  can be communicated to  $b$  (or vice-versa), the “locality loophole” is opened. Ensuring space-like separation between the choices and remote measurement events closes this loophole [13]. The “detection loophole” [5, 14] is opened by making the fair-sampling assumption, which says that a subset of the data can be used to represent the entire data set. This assumption is often used when some trials fail to produce outcomes due to inefficient detectors. High efficiency detectors are required to close the detection loophole and observe violation of the inequality [15]. The minimum detection efficiency required to close the detection loophole for the  $N$ th CBI experiment is given by Ref. [15] as

$$\eta_{\min}(N) = \frac{2}{\frac{N}{N-1} \cos\left(\frac{\pi}{2N}\right) + 1}, \quad (4)$$

assuming that the measurement efficiencies on  $a$  and  $b$  are equal and that a maximally entangled state is mea-

sured. This emphasizes the importance of high detection efficiency in large  $N$  CBI experiments. If the analysis of the data assumes that the outcomes of the trials are independent and identically distributed (i.i.d.), the “memory loophole” is opened [16]. For example, one way to determine  $I_N$  is by running each of the CBI setting pairs  $a_k b_l$  for a total number of  $M_{k,l}$  trials respectively and calculating

$$\bar{c}(a_l, b_k) = \frac{\sum_{i=1}^{M_{k,l}} c(x_i, y_i)}{M_{k,l}}, \quad (5)$$

(where  $i$  indexes the trials) to estimate each  $\mathcal{C}(a_l, b_k)$  term in Eq. (3). This analysis requires the i.i.d. assumption for standard error estimates to be valid. The memory loophole can be closed by applying appropriate analysis techniques to an experiment that uses randomized settings for each trial [17].

Previous experiments on the CBIs employed entangled photon pairs [9, 18–20]. The lowest yet reported upper bound on  $p_{\text{local}}$  is approximately 0.126 for  $N = 18$  [9], but this value is based on postselection for coincidences. All previous CBI experiments prior to our work with  $N \geq 3$  are open to locality, detection and memory loopholes.

Here, with a pair of atomic ions, we experimentally put an upper bound on  $p_{\text{local}}$  by measuring  $I_N$  with near 100 % detection efficiency. The measurement outcomes of every trial in each experiment are recorded and used to determine  $I_N$ , so the detection loophole is closed, as first incorporated in a CHSH Bell inequality experiment [21]. Furthermore, we address the memory loophole in a  $N = 6$  CBI experiment by employing uniformly random settings and developing a statistical analysis technique that does not require the assumption that trials are i.i.d. However, with each ion’s measurement inside the lightcone of the event where the other ion’s setting choice is made, we do not close the locality loophole. In a CBI experiment using atomic systems, the locality loophole could be closed by connecting distant ion traps with photonic links as demonstrated in [2, 22, 23].

Two beryllium ions ( ${}^9\text{Be}^+$ ) are confined and aligned along the axis of a linear Paul trap by applying a combination of radio frequency (RF) and static potentials [24] (see Fig. 2). This trap features segmented control electrodes allowing ions to be confined in different wells by applying controlled potentials [25]. The ions can be confined together in a single harmonic well, or separately confined in different locations along the trap axis. Time varying potentials are applied to the control electrodes to deterministically separate ions and transport them between different locations [25, 26].

The two states of the ions are encoded in the two electronic ground-state hyperfine levels  $|F = 2, m_F = 0\rangle = |\downarrow\rangle$  and  $|F = 1, m_F = 1\rangle = |\uparrow\rangle$ , where  $F$  and  $m_F$  are the total angular momentum and its projection along the quantization axis provided by an external magnetic field

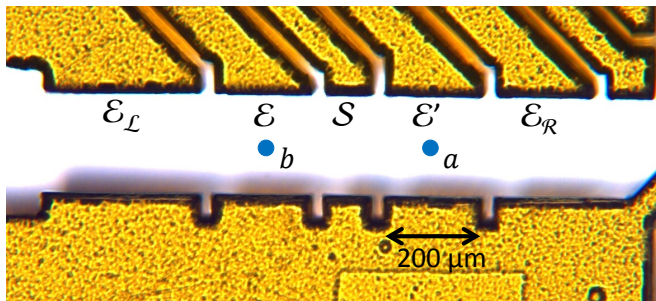


FIG. 2. Layout of the relevant segmented trap electrodes. Each CBI experiment begins with one ion located in zone  $\mathcal{E}$  and the other in zone  $\mathcal{E}'$ . The blue dots, which indicate the ions, are overlaid on a photograph showing the trap electrodes (gold). By transporting the ions in and out of zone  $\mathcal{S}$ , we individually implement settings and measure each ion sequentially (details in supplemental material). The ions are separated by at least  $\sim 340 \mu\text{m}$  when settings  $a_k b_l$  are applied, a distance much larger than the laser beams size of  $\sim 25 \mu\text{m}$ .

of  $\simeq 0.0119$ . For details, see Ref. [24] which includes an energy level diagram. The frequency splitting of the two states is approximately 1.2 GHz and is first-order insensitive to magnetic field fluctuations [27]. With coherent operations based on stimulated-Raman transitions (with laser wavelengths near 313 nm), we can deterministically create the entangled states

$$|\Phi_{+/-}\rangle = \frac{1}{\sqrt{2}} (|\uparrow\uparrow\rangle \pm |\downarrow\downarrow\rangle), \quad (6)$$

with high-fidelity, where the notation  $|\uparrow\uparrow\rangle$  denotes the two ion state  $|\uparrow\rangle_a |\uparrow\rangle_b$  [24] (see supplemental material for details on the Bell state generation). States  $|\Phi_{+/-}\rangle$  are created with the ions are located in zone  $\mathcal{S}$  (Fig. 2). This is followed by separating the ions and placing them in two separate potential wells, one located in zone  $\mathcal{E}$  and one located in  $\mathcal{E}'$ , separated by  $\sim 340 \mu\text{m}$ . These processes represent the source in Fig. 1 and prepare the two ions  $a$  and  $b$  for the measurement of  $I_N$  described below.

To implement the different settings, we illuminate the ions with stimulated-Raman-transition-inducing laser beams controlled with classical parameters. Ideally, they can be described as the following rotations:

$$\begin{aligned} |\uparrow\rangle_r &\rightarrow \frac{1}{\sqrt{2}} (|\uparrow\rangle_r - ie^{-ir_k} |\downarrow\rangle_r), \\ |\downarrow\rangle_r &\rightarrow \frac{1}{\sqrt{2}} (|\downarrow\rangle_r - ie^{ir_k} |\uparrow\rangle_r), \end{aligned} \quad (7)$$

where  $r = a$  or  $b$  to represent each of the ions, and the angles  $r_k = a_k$  or  $b_k$  are

$$a_k = \frac{(2k-1)\pi}{2N}, \quad (8)$$

$$b_l = -\frac{(l-1)\pi}{N}, \quad (9)$$

which are chosen from Eq. (2). These angles minimize the expected value of  $I_N$  if the produced entangled state is ideal [28]. These rotation operations are implemented by setting the amplitude and phase of the Raman laser beams with an acousto-optic modulator (AOM). The radio-frequency electric field driving the AOM is produced by a field-programmable gate array (FPGA)-controlled direct digital synthesizer. The classical variable is the phase of the oscillating field that implements a particular setting  $a_k$ . Analogous operations are applied to ion  $b$  with setting  $b_l$ . The laser beams implementing these rotations have a beam waist of  $\simeq 25 \mu\text{m}$  and are focused at zone  $\mathcal{S}$ . They are applied sequentially to one of the ions in zone  $\mathcal{S}$  while the other ion is located in a different well; each ion is transported in and out of zone  $\mathcal{S}$  to interact with the laser beams (see supplemental material).

After the settings rotations are applied, the state of each ion,  $|\uparrow\rangle$  or  $|\downarrow\rangle$  is measured sequentially in zone  $\mathcal{S}$  with a state-dependent fluorescence technique [29]. When the detection laser beam is applied, we detect on average 30 photon counts on a photomultiplier tube if the ion is in the  $|\uparrow\rangle$  state and about 2 counts if the ion is in the  $|\downarrow\rangle$  state. Our photon collection apparatus images ions in zone  $\mathcal{S}$  with a field of view of approximately  $50 \mu\text{m}$ . We label a measurement outcome “dark” ( $D$ ) if 6 or fewer photons are observed and “bright” ( $B$ ) if more than 6 are observed. Thus we obtain the 4 possible joint-measurement fluorescence outcomes  $BB, BD, DB, DD$ , for each trial. These outcomes correspond to the states  $|\uparrow\uparrow\rangle, |\uparrow\downarrow\rangle, |\downarrow\uparrow\rangle, \text{ and } |\downarrow\downarrow\rangle$ . Among previous CHSH-type experiments with trapped ions [21–23, 30], only two were performed with ions manipulated and measured in individual wells [22, 23]. In those experiments the ions were confined in two traps separated by about  $\sim 1 \text{ m}$ .

When the state  $|\Phi_+\rangle$  is prepared, we compute an estimate  $\hat{I}_N$  of  $I_N$  as shown in Eq. (3) with Eq. (5) used to estimate the  $\bar{\mathcal{C}}(a_k, b_l)$  terms. For the state  $|\Phi_-\rangle$  we instead use anticorrelations and compute

$$\begin{aligned} \hat{I}_N^A &= \bar{\mathcal{A}}(a_1, b_1) + \bar{\mathcal{A}}(a_1, b_2) + \bar{\mathcal{A}}(a_2, b_2) + \dots \\ &\dots + \bar{\mathcal{A}}(a_N, b_N) + (1 - \bar{\mathcal{A}}(a_N, b_1)), \end{aligned} \quad (10)$$

where  $\bar{\mathcal{A}}(a_k, b_l) = 1 - \bar{\mathcal{C}}(a_k, b_l)$ . The measured  $\hat{I}_N^A$  is equivalent to  $\hat{I}_N$  for the purpose of quantifying  $p_{\text{local}}$ .

We performed the experiment for the CBI parameter  $N$  ranging from 2 to 15. Two different data sets, collected  $\sim 6$  months apart, were obtained. Figure 3 shows the experimentally obtained CBI parameter  $\hat{I}_N$  as a function of  $N$ . The data points in Fig. 3 were obtained with multiple sequential trials having the same settings, then iterated across different choices of settings. The error bars are calculated under the assumption that the settings and outcomes are i.i.d. The error bars indicate the propagated standard errors  $\sqrt{\sum_j \epsilon_j^2}$ ,

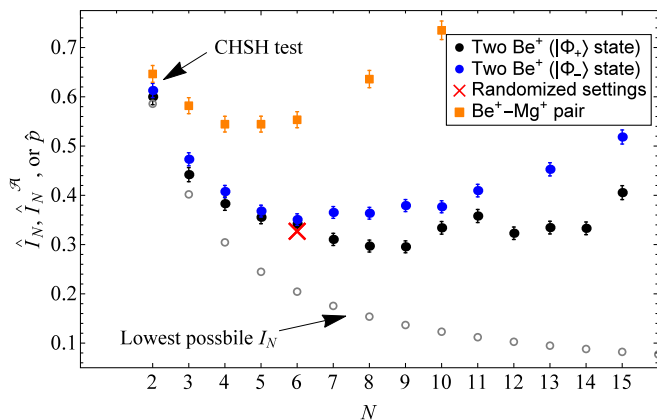


FIG. 3. Experimentally measured values  $\hat{I}_N$  and  $\hat{I}_N^A$  as a function of  $N$ . Data represented by black and blue dots are obtained with two  ${}^9\text{Be}^+$  ions, with black (blue) dots corresponds to tests on  $|\Phi_+\rangle$  ( $|\Phi_-\rangle$ ). These two data sets were obtained approximately six months apart. The difference between them and the finer features within each data set are probably due to miscalibrations and our inability to reproduce exact experimental conditions. Orange squares are data from tests on  $|\Phi_+\rangle$  prepared on a  ${}^9\text{Be}^+ \text{-} {}^{25}\text{Mg}^+$  pair. The red cross represents the (95 % confidence level) upper bound  $\hat{p} = 0.327$ , estimated using our statistical framework, which does not require the i.i.d. assumption. The gray circles indicate the lowest  $I_N$  achievable with perfect CBI experiments using a maximally entangled state. As  $N$  increases from 2, the experimentally measured values of  $\hat{I}_N$  for each different pair of ions reach a minimum and then trend upward. This is due to errors that accumulate during experiments with higher values of  $N$ . In general,  $\hat{I}_N$  becomes more sensitive to errors and noise as  $N$  increases [15].

with  $\epsilon_j = \sqrt{\chi_j(1 - \chi_j)/(M_j - 1)}$  where  $M_j$  is the number of trials (here  $M_j \sim 2,000$ ) and  $\chi_j$  is the averaged correlated or anticorrelated outcome for the  $j$ th setting pair. The  $\hat{I}_2$  experiment took a total of  $\sim 5$  minutes, the one for  $\hat{I}_{15} \sim 20$  minutes. The lowest value of  $\hat{I}_N$  is obtained for the  $N = 9$  data run, which corresponds to  $\hat{I}_9 = 0.296(12)$ .

To remove the i.i.d. assumption, we performed an  $N = 6$  experiment employing uniformly random settings. The settings were chosen with a pseudo-random generator during run time. For each randomly chosen setting pair, blocks of 100 trials with identical settings were carried out before changing to the next randomly selected setting pair. This procedure was repeated 1,398 times. This is the number of blocks we obtained in a single day's experiment run and was deemed sufficient for our statistical analysis to be reasonably informative. While we could have run one trial per settings choice, this would have implied a low data collection efficiency since a single trial takes  $\sim 10$  ms, but reprogramming the FPGA controlling the apparatus to change the settings takes  $\sim 4$  s. This  $N = 6$  experiment took  $\sim 7$  hours. Although 100 outcome pairs are available for each random settings

choice, only a single trial from each block should be analyzed when not making the i.i.d. assumption. We chose ahead of time to use the center trial (the 50th trial of each block) in our analysis. The choice of the 50th trial was arbitrary; any other choice would have also produced a valid analysis. To enable this choice, we assume that the 50th trial does not depend on the earlier trials in each block. Collisions between ions and background gases can cause the ions to overheat or be ejected from the potential well. To reduce the consequences of these effects, we checked the status of the ions with fluorescence measurements. If the measurements made prior to the beginning of each trial do not detect a problem with the ions, that trial was “heralded” and included in the analysis (see supplemental material). Because we use only information gained prior to the beginning of a trial to herald that trial, the detection loophole is not opened. When studying the 50th trial of each block, 1,361 trials were therefore analyzed.

A memory-robust statistical framework is formulated to infer a bound on the maximum local content in the observed correlation. For  $|\Phi_+\rangle$ , we draw inferences based on the statistic  $T_i(x, y, a_k, b_l)$ , defined as

$$T_i(x, y, a_k, b_l) = \begin{cases} 0 & \text{if } x = y \text{ and } (a_k, b_l) \neq (a_N, b_1) \\ 1 & \text{if } x \neq y \text{ and } (a_k, b_l) \neq (a_N, b_1) \\ 1 & \text{if } x = y \text{ and } (a_k, b_l) = (a_N, b_1) \\ 0 & \text{if } x \neq y \text{ and } (a_k, b_l) = (a_N, b_1) \end{cases}, \quad (11)$$

where  $x$  and  $y$  are the measurement outcomes from the two ions when they are measured with settings  $a_k b_l$  chosen from Eq. (2) during trial  $i$ . As a trial-by-trial function of both settings and outcomes,  $T_i$  is more suitable for memory-robust statistical analysis than a statistic (such as  $\bar{C}$ ) that is normalized by the number of times each measurement setting occurs [16]. The expectation value of  $T_i$  is  $1 - I_N/(2N)$ , so intuitively larger values of  $\sum_{i=1}^{1,361} T_i$  should correspond to a lower local fraction  $P^L$  in Eq. (1). In the presence of memory effects, it is possible for the proportion of local states to change over time. Hence we model each trial  $i$  as having a probability  $p_{\text{local}}^i$  of generating a local state, and derive a one-sided  $1 - \alpha$  confidence interval  $[0, \hat{p}]$  for  $p_{\text{local}}^{\min} := \min_i p_{\text{local}}^i$ , the minimum local content that can occur over the course of the experiment. The probability of seeing a  $\sum_{i=1}^n T_i$  statistic as large or larger than that actually observed for a model with  $p_{\text{local}}^{\min} = q$  is less than or equal to the same probability for an i.i.d. model with  $p_{\text{local}}^i = q$  for all  $i$ . From this, the desired confidence interval can be obtained by inversion of hypothesis-test acceptance regions (§7.1.2 of [31]); see the supplemental material. In particular, this implies that we can take  $\hat{p}$  to be the largest value  $x$  for which a binomial random variable with  $n = 1,361$  trials and probability of success  $(2N - x)/2N$  yields a value as great or greater than the observed value of  $\sum_i T_i$  with a

probability of at least  $\alpha$ .

We compute one-sided  $p_{\text{local}}^{\text{min}}$  confidence intervals of  $[0, 0.327]$ ,  $[0, 0.366]$ , and  $[0, 0.413]$  for confidence levels of 0.95, 0.99, and 0.999, respectively, using the 50th trial in each block of the randomized  $N = 6$  experiment. Randomization of settings and the use of this statistical framework also remove any concern that experimental drifts might erroneously lead to a lower estimate of  $p_{\text{local}}^{\text{min}}$ .

The values of  $\hat{I}_6$  and  $\hat{p}$  obtained when we analyzed the 1st through 100th trial in each block, representing the  $I_6$  estimates and confidence intervals that would have been obtained with a different choice of representative trial, are shown in the supplemental material.

Using the same apparatus, we also perform the CBI experiment on a pair of  ${}^9\text{Be}^+$  and  ${}^{25}\text{Mg}^+$  ions; see Ref. [32] and supplementary material for details. The computed  $\hat{I}_N$  values are shown as orange squares in Fig. 3.

Our lowest measurement of  $\hat{I}_2$  corresponds to a CHSH inequality parameter (sum of correlations) of  $B_{\text{CHSH}} = 2.80(2)$ . Under local-realism  $B_{\text{CHSH}} = 4 - 2I_2 \leq 2$ . A consequence of the near-maximal violations of the CHSH inequality ( $B_{\text{CHSH}}^{\text{max}} = 2\sqrt{2} \simeq 2.82$ ) provides a black box certification of the created entangled states [33–35]. Such a characterization with minimal assumptions on our physical system and measurements is formalized by the self-testing framework [36, 37]. Using the method of Ref. [34], we infer a self-tested Bell-state fidelity lower bound (at the 95 % confidence level) of  $\sim 0.958$ . This is a record self-tested Bell-state fidelity with the detection loophole closed; see supplementary material for comparison with the experiments reported in Refs. [21–23, 30, 32, 38–43].

The apparatus used here is designed for the implementation of quantum information processing (QIP) with trapped-ions in a scalable system of trap zones in an array [44, 45]. The basic QIP elements incorporated for the realization of the CBI experiment described here include high-fidelity state preparation, manipulation, and measurement on individual qubits with long coherence times, transport between zones, and high-fidelity two-qubit gates. Therefore, CBI experimental results can also be regarded as a useful benchmark toward the goal of general purpose scalable QIP.

Our experiment is the first to report violation of CBIs for  $N \geq 3$  while closing the detection loophole. Also, it is the first CBI for  $N \geq 3$  experiment that uses massive particles. We infer the presence of distributions whose local fraction was less than 0.327 at the 95 % confidence level. Furthermore, for the special case of the CHSH inequality, our self-tested fidelity appears to be the highest for a deterministically created Bell state.

This work was supported by the Office of the Director of National Intelligence (ODNI) Intelligence Advanced Research Projects Activity (IARPA), ONR and the NIST Quantum Information Program. We thank L. Shalm and

J. Bergquist for helpful suggestions on the manuscript. We express gratitude to J. P. Gaebler, Y. Lin, R. Jördens, R. Bowler, and A. C. Wilson for contributing to the experimental setup. S. Erickson is supported by the National Science Foundation Graduate Research Fellowship under Grant no. DGE 1650115. D. Kienzler acknowledges support from the Swiss National Science Foundation under grant no. 165208. This manuscript is a contribution of NIST and not subject to U.S. copyright.

---

\* tingrei.tan@nus.edu.sg; Curent address: Centre for Quantum Technologies, National University of Singapore, 3 Science Drive 2, 117543 Singapore

† david.wineland@nist.gov

- [1] J. S. Bell, “On the EPR Paradox,” *Physics* **1** 195 (1964).
- [2] B. Hensen *et al.*, “Loophole-free Bell inequality violation using electron spins separated by 1.3 kilometers,” *Nature* **526**, 682 (2015).
- [3] L. K. Shalm *et al.*, “Strong loophole-free test of local realism,” *Phys. Rev. Lett.* **115** 250402 (2015).
- [4] M. Giustina *et al.*, “Significant-loophole-free test of Bell’s theorem with entangled photons,” *Phys. Rev. Lett.* **115** 250401 (2015).
- [5] P. M. Pearle, “Hidden-variable example based upon data rejection,” *Phys. Rev. D* **2**, 1418 (1970).
- [6] A. C. Elitzur, S. Popescu, and D. Rohrlich, “Quantum nonlocality for each pair in an ensemble,” *Phys. Lett. A* **162**, 25 (1992).
- [7] J. F. Clauser, M. A. Horne, A. Shimony, and R. A. Holt, “Proposed experiment to test local hidden-variable theories,” *Phys. Rev. Lett.* **23**, 880 (1969).
- [8] J. Barrett, A. Kent, and S. Pironio, “Maximally nonlocal and monogamous quantum correlations,” *Phys. Rev. Lett.* **97**, 170409 (2006).
- [9] B. G. Christensen, Y.-C. Liang, N. Brunner, N. Gisin, and P. Kwiat, “Exploring the limits of quantum nonlocality with entangled photons,” *Phys. Rev. X* **5**, 041052 (2015).
- [10] P. Bierhorst, “Geometric decompositions of Bell polytopes with practical applications,” *J. Phys. A: Math. Theor.* **49** 215301 (2016).
- [11] N. Brunner, D. Cavalcanti, S. Pironio, V. Scarani, and S. Wehner, “Bell nonlocality,” *Rev. Mod. Phys.* **86**, 419 (2014).
- [12] J.-Å. Larsson, “Loopholes in Bell inequality tests of local realism,” *J. Phys. A* **47** 424003 (2014).
- [13] J. S. Bell, J. F. Clauser, M. A. Horne, and A. Shimony, “An exchange on local beables,” *Dialectica* **39** 85 (1985).
- [14] J. F. Clauser and M. A. Horne, “Experimental consequences of objective local theories,” *Phys. Rev. D* **10**, 526 (1974).
- [15] A. Cabello, J.-Å. Larsson, and D. Rodriguez, “Minimum detection efficiency required for a loophole-free violation of the Braunstein-Caves chained Bell inequalities,” *Phys. Rev. A* **79** 062109 (2009).
- [16] J. Barrett, D. Collins, L. Hardy, A. Kent, and S. Popescu, “Quantum nonlocality, Bell inequalities, and the memory loophole,” *Phys. Rev. A* **66**, 042111 (2002).
- [17] R. D. Gill, in *Mathematical Statistics and Applications:*

- Festschrift for Constance van Eeden*, edited by M. Moore, S. Froda, and L. Léger (Institute of Mathematical Statistics, Beachwood, Ohio, 2003), Vol. 42, pp. 133-154.
- [18] E. Pomarico, J.-D. Bancal, B. Sanguinetti, A. Rochdi, and N. Gisin, “Various quantum nonlocality tests with a commercial two-photon entanglement source,” *Phys. Rev. A* **83**, 052104 (2011).
- [19] L. Aolita *et al.*, “Fully nonlocal quantum correlations,” *Phys. Rev. A* **85**, 032107 (2012).
- [20] T. E. Stuart, J. A. Slater, R. Colbeck, R. Renner, and W. Tittel, “Experimental bound on the maximum predictive power of physical theories,” *Phys. Rev. Lett.* **109**, 020402 (2012).
- [21] M. A. Rowe *et al.*, “Experimental violation of a Bell’s inequality with efficient detection,” *Nature* **409** 791 (2001).
- [22] D. N. Matsukevich, P. Maunz, D. L. Moehring, S. Olmschencck, and C. Monroe, “Bell inequality violation with two remote atomic qubits,” *Phys. Rev. Lett.* **100**, 150404 (2008).
- [23] S. Pironio, *et al.*, “Random numbers certified by Bell’s theorem,” *Nature* **464**, 1021 (2010).
- [24] J. P. Gaebler *et al.*, “High-fidelity universal gate set for  ${}^9\text{Be}^+$  ion qubits,” *Phys. Rev. Lett.* **117**, 060505 (2016).
- [25] R. B. Blakestad *et al.*, “Near-ground-state transport of trapped-ion qubits through a multidimensional array,” *Phys. Rev. A* **84**, 032314 (2011).
- [26] R. Bowler *et al.*, “Coherent diabatic ion transport and separation in a multizone trap array,” *Phys. Rev. Lett.* **109**, 080502 (2012).
- [27] C. Langer *et al.*, “Long-lived qubit memory using atomic ions,” *Phys. Rev. Lett.* **95**, 060502 (2005).
- [28] S. L. Braunstein and C. M. Caves, “Wringing out better Bell inequalities,” *Ann. Phys. (N. Y.)* **202**, 22 (1990).
- [29] R. Blatt and P. Zoller, “Quantum jumps in atomic systems,” *Eur. J. Phys.* **9**, 250 (1988).
- [30] C. J. Ballance *et al.*, “Hybrid quantum logic and a test of Bell’s inequality using two different atomic isotopes,” *Nature* **528**, 384 (2015).
- [31] J. Shao. *Mathematical Statistics*. Springer, New York, 2nd edition (2013).
- [32] T. R. Tan *et al.*, “Multi-element logic gates for trapped-ion qubits,” *Nature* **528**, 380 (2015).
- [33] J. -D. Bancal, M. Navascués, V. Scarani, T. Vértesi, and T. H. Yang, “Physical characterization of quantum devices from nonlocal correlations,” *Phys. Rev. A* **91**, 022115 (2015).
- [34] J. Kaniewski, “Analytic and nearly optimal self-testing bounds for the Clauser-Holt-Shimony-Horne and Mermin inequalities,” *Phys. Rev. Lett.* **117**, 070402 (2016).
- [35] C.-E. Bardyn, T. C. H. Liew, S. Massar, M. McKague, and V. Scarani, “Device-independent state estimation based on Bell’s inequalities,” *Phys. Rev. A* **80**, 062327 (2009).
- [36] D. Mayers and A. Yao, “Self testing quantum apparatus,” *Quantum Inf. Comput.* **4**, 273 (2004).
- [37] M. McKague, T. H. Yang, and V. Scarani, “Robust self-testing of the singlet,” *J. Phys. A* **45**, 455304 (2012).
- [38] M. Ansmann *et al.*, “Violation of Bell’s inequality in Josephson phase qubits,” *Nature* **461**, 504 (2009).
- [39] J. Hofmann *et al.*, “Heralded Entanglement Between Widely Separated Atoms,” *Science* **337**, 72 (2012).
- [40] W. Pfaff *et al.*, “Demonstration of entanglement-by-measurement of solid-state qubits,” *Nature Physics* **9**, 29 (2013).
- [41] B. Vlastakis *et al.*, “Characterizing entanglement of an artificial atom and a cavity cat state with Bell’s inequality,” *Nature Communications* **6**, 8970 (2015).
- [42] J. P. Dehollain *et al.*, “Bell’s inequality violation with spins in silicon,” *Nature Nanotechnology* **11**, 242 (2016).
- [43] B. Hensen *et al.*, “Loophole-free Bell test using electron spins in diamond: second experiment and additional analysis,” *Scientific Reports* **6**, 30289 (2016).
- [44] D. J. Wineland *et al.*, “Experimental issues in coherent quantum-state manipulation of trapped atomic ions,” *J. Res. Natl. Inst. Stand. Technol.* **103**, 259 (1998).
- [45] D. Kielpinski, C. Monroe, and D. J. Wineland, “Architecture for a large-scale ion trap quantum computer,” *Nature* **417**, 709 - 711 (2002).
- [46] A. Sørensen and K. Mølmer, “Quantum computation with ions in thermal motion,” *Phys. Rev. Lett.* **82**, 1971 (1999).
- [47] P. J. Lee *et al.*, “Phase control of trapped ion quantum gates,” *J. Opt. B* **7**, S371 (2005).
- [48] C. A. Sackett *et al.*, “Experimental entanglement of four particles,” *Nature* **404**, 256 (2000).
- [49] R. Ozeri *et al.*, “Errors in trapped-ion quantum gates due to spontaneous photon scattering,” *Phys. Rev. A* **75**, 042329 (2007).
- [50] Q. A. Turchette *et al.*, “Heating of trapped ions from the quantum ground state,” *Phys. Rev. A* **61**, 063418 (2000).
- [51] P. Bierhorst, “A robust mathematical model for a loophole-free Clauser-Horne experiment,” *J. Phys. A: Math. Theor.* **48** 195302 (2015).